Small-conductance Ca^{2+}-activated K^+ channels promote J-wave syndrome and phase 2 reentry

Julian Landaw, PhD,[*1] Zhaoyang Zhang, PhD,[*1] Zhen Song, PhD,[*] Michael B. Liu, PhD,[*] Riccardo Olcese, PhD,[†‡] Peng-Sheng Chen, MD, FHRS,[§] James N. Weiss, MD,[*‡] Zhilin Qu, PhD[*‖]

*From the *Department of Medicine, David Geffen School of Medicine, University of California, Los Angeles, Los Angeles, California, †Department of Anesthesiology and Perioperative Medicine, David Geffen School of Medicine, University of California, Los Angeles, Los Angeles, California, ‡Department of Physiology, David Geffen School of Medicine, University of California, Los Angeles, Los Angeles, California, §Krannert Institute of Cardiology and Division of Cardiology, Department of Medicine, Indiana University School of Medicine, Indianapolis, Indiana, and ‖Department of Computational Medicine, David Geffen School of Medicine, University of California, Los Angeles, Los Angeles, California.*

BACKGROUND Small-conductance Ca^{2+}-activated potassium (SK) channels play complex roles in cardiac arrhythmogenesis. SK channels colocalize with L-type Ca^{2+} channels, yet how this colocalization affects cardiac arrhythmogenesis is unknown.

OBJECTIVE The purpose of this study was to investigate the role of colocalization of SK channels with L-type Ca^{2+} channels in promoting J-wave syndrome and ventricular arrhythmias.

METHODS We carried out computer simulations of single-cell and tissue models. SK channels in the model were assigned to preferentially sense Ca^{2+} in the bulk cytosol, subsarcolemmal space, or junctional cleft.

RESULTS When SK channels sense Ca^{2+} in the bulk cytosol, the SK current (I_{SK}) rises and decays slowly during an action potential, the action potential duration (APD) decreases as the maximum conductance increases, no complex APD dynamics and phase 2 reentry can be induced by I_{SK}. When SK channels sense Ca^{2+} in the subsarcolemmal space or junctional cleft, I_{SK} can rise and decay rapidly during an action potential in a spike-like pattern because of spiky Ca^{2+} transients in these compartments, which can cause spike-and-dome action potential morphology, APD alternans, J-wave elevation, and phase 2 reentry. Our results can account for the experimental finding that activation of I_{SK} induced J-wave syndrome and phase 2 reentry in rabbit hearts.

CONCLUSION Colocalization of SK channels with L-type Ca^{2+} channels so that they preferentially sense Ca^{2+} in the subsarcolemmal or junctional space may result in a spiky I_{SK}, which can functionally play a similar role of the transient outward K^+ current in promoting J-wave syndrome and ventricular arrhythmias.

KEYWORDS Alternans; Computer modeling; J-wave syndrome; Phase 2 reentry; SK channel

(Heart Rhythm 2020;17:1582–1590)

Introduction

Small-conductance Ca^{2+}-activated K^+ (SK) channels are widely expressed in a variety of cell types and play multiple biological roles, particularly in the nervous system where they regulate neuronal firing.[1] The SK current (I_{SK}) is also present in atrial and ventricular myocytes under normal and diseased conditions.[2–9] Depending on experimental conditions, both proarrhythmic and antiarrhythmic effects of I_{SK} have been identified in experiments using apamin, a selective SK channel blocker. However, the underlying mechanisms are not well understood.

I_{SK} is activated by intracellular Ca^{2+} with a fast time constant on the order of a few milliseconds,[10–13] and thus its rising and decaying time course tracks the intracellular Ca^{2+} transient. Moreover, studies have found that SK channels colocalize with L-type Ca^{2+} channels (LCCs) in ventricular myocytes[4,5,7] such that SK channels may be transiently exposed to a much higher Ca^{2+} concentrations in the

This work was supported by the National Institutes of Health under grants no. R01 HL139829 (to Drs Chen and Qu), R01 HL134709 (to Dr Qu), R01 HL134346 (to Dr Olcese), and T32-GM008185 (to Drs Landaw and Liu), F30 HL140864 (to Dr Landaw), and F30 HL132449 (to Dr Liu); the Laubisch and Kawata Endowments of UCLA (to Dr Weiss); a Medtronic-Zipes Endowment of the Indiana University (to Dr Chen); and the Natural Science Foundation of Ningbo, China, under grant no. 2017A610142 (to Dr Zhang). [1]Drs Landaw and Zhang contributed equally to this work. **Address reprint requests and correspondence:** Dr Zhilin Qu, Division of Cardiology, Department of Medicine, David Geffen School of Medicine, University of California, Los Angeles, A2-237 CHS, 650 Charles E Young Drive S, Los Angeles, CA 90095. E-mail address: zqu@mednet.ucla.edu.

1547-5271/$-see front matter https://doi.org/10.1016/j.hrthm.2020.04.023

submembrane space when the nearby LCCs and ryanodine receptors open. This may make I_{SK} a transient current, similar to the transient outward K^+ current (I_{to}). In agreement with this view, a spike-like I_{SK} has been observed in ventricular myocytes under voltage clamp conditions.[7,14] In a recent experimental study, Chen et al[15] discovered that rabbit hearts exposed to a drug that activates I_{SK} while simultaneously inhibiting the Na^+ current developed J-wave syndrome leading to phase 2 reentry (P2R) and ventricular arrhythmias. Since I_{to}, the current most commonly implicated in P2R, is small in rabbits at normal heart rates, we hypothesized that the arrhythmogenic J-wave syndrome in rabbit hearts was related to the I_{to}-like properties of the activated I_{SK}.

To test this hypothesis, we carried out computer simulations of single myocyte and 1-dimensional (1D) cable models to investigate the effects of I_{SK} and its subcellular localization on action potential (AP) morphology and P2R. In single myocytes, we investigated the influence of the subcellular localization of SK channels on AP morphology and complex action potential duration (APD) dynamics. In 1D cable simulations, we simulated the effects of I_{SK} and its subcellular localization on J-wave properties and P2R. Our main conclusion is that colocalization of SK channels with LCCs results in I_{SK} properties that can result in J-wave syndrome and potentiate ventricular arrhythmias via promoting T-wave alternans and P2R.

Methods

Modeling I_{SK}

Komendantov et al[16] used an I_{SK} formulation to study neuronal firing as follows:

$$I_{SK} = G_{SK}\frac{1}{1+(K_d/[Ca])^4}(V - E_K) \quad (1)$$

Here we modified the I_{SK} formulation of Komendantov et al to include a time-dependent gating variable; that is,

$$I_{SK} = G_{SK}x_{SK}(V - E_K) \quad (2)$$

where G_{SK} is the maximum conductance and E_K the K^+ reversal potential. x_{SK} is the time-dependent gating variable described by

$$\frac{dx_{SK}}{dt} = \frac{X_{SK,\infty} - X_{SK}}{\tau_{SK}}$$

where $x_{SK,\infty}$ is a Hill function of Ca^{2+}; that is,

$$x_{SK,\infty} = \frac{1}{1+(K_d/[Ca]_{SK})^n} \quad (4)$$

where $[Ca^{2+}]_{SK}$ is the Ca^{2+} concentration sensed by SK channels. In Equation 4, n is the Hill coefficient, which we set at n = 4, in the range from 2 to 6 as measured in experiments.[3,10,13,17] Thus when $\tau_{SK} = 0$, Equation 2 is identical to Equation 1. The reported experimental K_d is in the submicromolar range.[3,10–13,17] For example, Chua et al[3] found K_d = 0.5 μM for normal ventricles and K_d = 0.3 μM for failing ventricles. However, we will use different K_d values for different SK localizations, as discussed in more detail in the Discussion section.

As for τ_{SK}, we plotted experimental data in Figure 1 from different experiments (in different symbols).[10–13] Using their multistate Markovian SK channel model, Hirschberg et al[10] showed that τ_{SK} exhibits an inverse linear relationship with $[Ca^{2+}]$. In other words, τ_{SK} can be represented by a Hill function with a Hill coefficient of 1. On the basis of this observation, we formulated τ_{SK} as

$$\tau_{SK} = \tau_0 + \frac{\tau_1}{1+([Ca]_{SK}/0.1)} \quad (5)$$

A plot of this function for $\tau_0 = 4$ and $\tau_1 = 20$ is shown in Figure 1, which is well within the range of the experimental data.

In this study, we used the Shannon-Bers rabbit ventricular AP model,[18] which has 3 cytosolic Ca^{2+} compartments: bulk cytosolic compartment, subsarcolemmal compartment, and junctional cleft. The corresponding Ca^{2+} concentrations in the 3 compartments are abbreviated as $[Ca^{2+}]_i$, $[Ca^{2+}]_{SL}$, and $[Ca^{2+}]_{jct}$, respectively. These concentrations will be used for $[Ca^{2+}]_{SK}$ in Equations 4 and 5 when SK channels sense Ca^{2+} in different compartments.

Single-cell model

Simulations of single cells were carried out using the following differential equation:

$$C_m\frac{dV}{dt} = -I_{ion} + I_{sti} \quad (6)$$

where V is the voltage and C_m = 1 μF/cm^2 is the membrane capacitance. The ionic current I_{ion} was from the Shannon-Bers rabbit ventricular AP model,[18] with the original Matlab code downloaded from the Web site https://somapp.ucdmc.ucdavis.edu/Pharmacology/bers/.

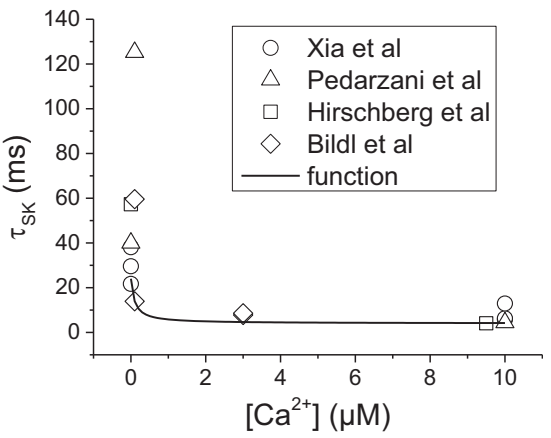

Figure 1 Activation time constant (τ_{SK}) vs intracellular calcium concentration ($[Ca^{2+}]$). Different symbols are data from different experiments.[10–13] The line is a plot of the mathematical model equation 6 with τ_0 = 4 ms and τ_1 = 20 ms.

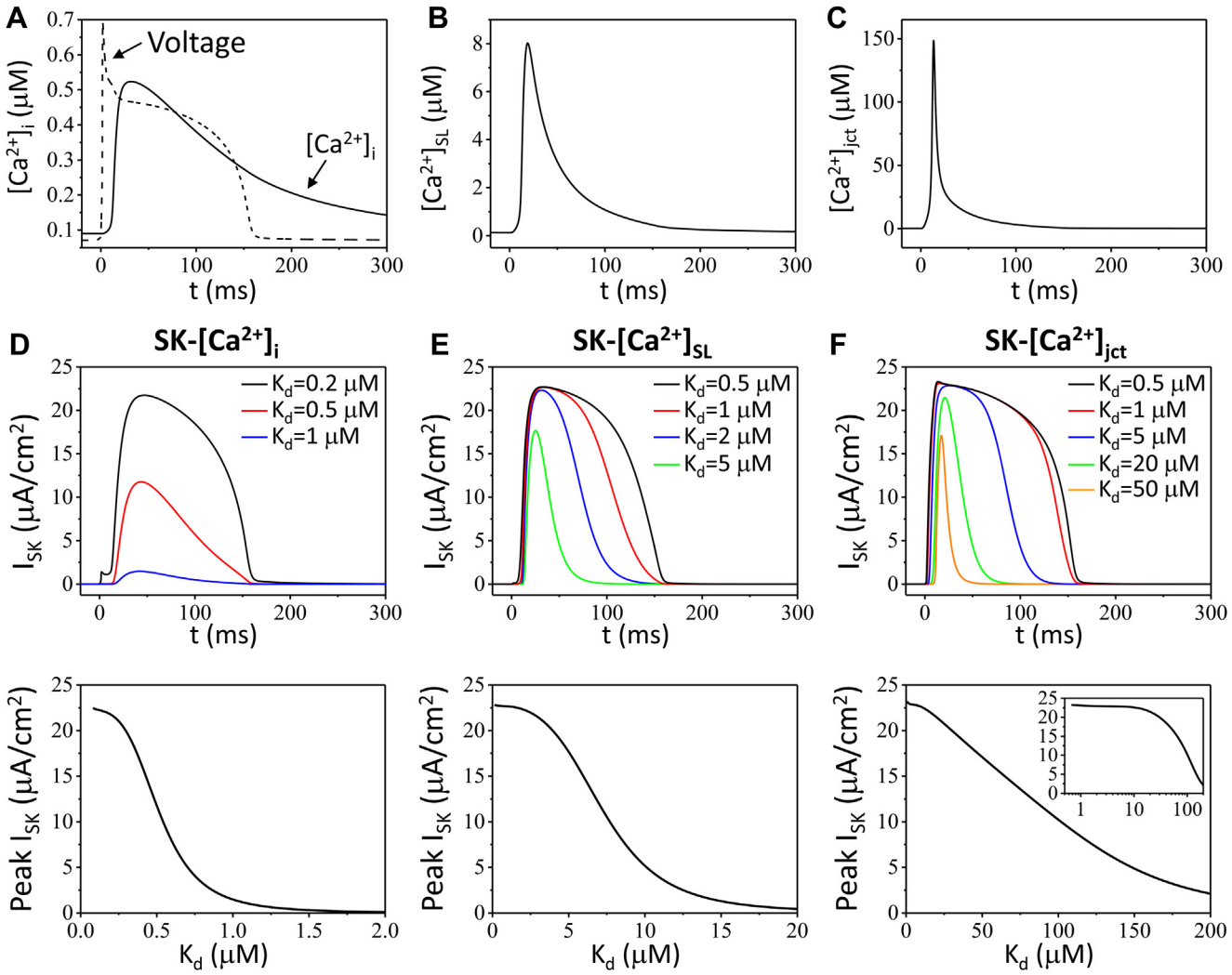

Figure 2 Ca^{2+} transients in different compartments of the Shannon-Bers model and dependence of I_{SK} properties on SK channel localization. **A:** The *dashed line* denotes the AP in the Shannon-Bers rabbit ventricular AP model.[18] The *solid line* denotes the bulk cytosolic Ca^{2+} concentration ($[Ca^{2+}]_i$) during the AP. **B:** Subsarcolemmal Ca^{2+} concentration ($[Ca^{2+}]_{SL}$) during the AP. **C:** Junctional Ca^{2+} concentration ($[Ca^{2+}]_{jct}$) during the AP. **D:** I_{SK} under an AP clamp condition using the AP in panel A for different K_d values when SK channels sense the bulk cytosolic Ca^{2+} (labeled as SK-$[Ca^{2+}]_i$). **E:** Same as panel A when SK channels sense the subsarcolemmal Ca^{2+} (labeled as SK-$[Ca^{2+}]_{SL}$). **F:** Same as panel A when SK channels sense the junctional Ca^{2+} (labeled as SK-$[Ca^{2+}]_{jct}$). G_{SK} = 0.25 pS/pF; Ca^{2+} =calcium; AP=action potential; SK=small-conductance Ca^{2+} -activated K^+; I_{SK}=SK current; G_{SK}=maximum conductance of I_{SK}.

1D cable model

1D cables were described by the following partial differential equation for voltage:

$$\frac{\partial V}{\partial t} = -\frac{I_{ion}}{C_m} + D\frac{\partial^2 V}{\partial x^2} \tag{7}$$

where D = 0.001 cm^2/ms is the diffusion constant describing the strength of gap junction coupling. The pseudo-electrocardiogram (ECG) was calculated as follows:

$$\text{Pseudo-ECG} = \int_0^{3\ \text{cm}} D\nabla V \cdot \nabla\left(\frac{1}{r}\right) dx \tag{8}$$

where $r = \sqrt{(x - x_p)^2 + y_p^2}$ and x is a point in the cable and (x_p, y_p) = (2.28 cm, 1 cm) is the location of the pseudo-ECG electrode.

Numerical methods

Single cell simulations were performed using a forward Euler method with a fixed time step Δt = 0.005 ms. 1D cable simulations were performed using CUDA, a programming language designed for graphical processing units, and a forward Euler method with a fixed time step Δt = 0.005 ms. The cable consists of 200 cells, and the cell length corresponding to the spatial step is Δx = 0.015 cm. No-flux boundary conditions were used.

Results

SK channel localization and I_{SK} properties

Figures 2A–2C show an AP and the corresponding Ca^{2+} transients from different cytosolic compartments of the Shannon-Bers model. The bulk cytosolic Ca^{2+} transient peaks at 0.5 μM (Figure 2A), the subsarcolemmal Ca^{2+}

peaks at 8 μM and becomes spikier (Figure 2B), and the junctional Ca^{2+} reaches as high as 150 μM and is much spikier (Figure 2C). We then investigated the effects of SK channel localization on I_{SK} properties under an AP clamp condition using the AP waveform in Figure 2A. Figures 2D–2F show I_{SK} vs time for different K_d values (upper panels) and peak I_{SK} vs K_d (lower panels) for SK channels sensing Ca^{2+} in different compartments, labeled as SK-$[Ca^{2+}]_i$, SK-$[Ca^{2+}]_{SL}$, and SK-$[Ca^{2+}]_{jct}$, respectively. When SK channels sense Ca^{2+} in the bulk cytosolic compartment, I_{SK} is broad and the amplitude decreases by half when K_d increases to 0.5 μM. When SK channels sense Ca^{2+} in the subsarcolemmal compartment, I_{SK} is broad when K_d is low but becomes narrower as K_d increases. The amplitude of I_{SK} does not decrease until K_d reaches 2 μM and by half when K_d increases to 7.5 μM. When SK channels sense Ca^{2+} in the junctional cleft, I_{SK} behaves similarly to when SK channels sense Ca^{2+} in the subsarcolemmal compartment. However, a much higher K_d is required. The amplitude of I_{SK} does not decrease until K_d increases to 10 μM and by half when K_d increases to 90 μM. Note that the current densities and width of the current profiles in Figures 2E and 2F are in the same ranges as the experimental data shown by Terentyev and coworkers.[7,14]

Effects of I_{SK} on AP morphology

We next carried out simulations to show how I_{SK} properties affect AP morphology (Figure 3). When K_d is low (upper panels in Figure 3), increasing G_{SK} shortens APD and the AP becomes more and more triangular for SK channels that sense Ca^{2+} in any 1 of the 3 compartments. When SK channels sense Ca^{2+} in the bulk cytosolic compartment, changing K_d does not change the AP properties. However, when SK channels sense Ca^{2+} in the subsarcolemmal compartment or junctional cleft, spike-and-dome morphology and lengthening of APD occur when G_{SK} was increased to a certain value. When G_{SK} increases further, APD suddenly shortens to a short value. These AP behaviors are the same as those induced by I_{to} as shown in many of the previous studies.[19–21]

I_{SK} promotes APD alternans and chaos

We examined the effects and the subcellular localization of SK channels on APD dynamics (Figure 4). When K_d is

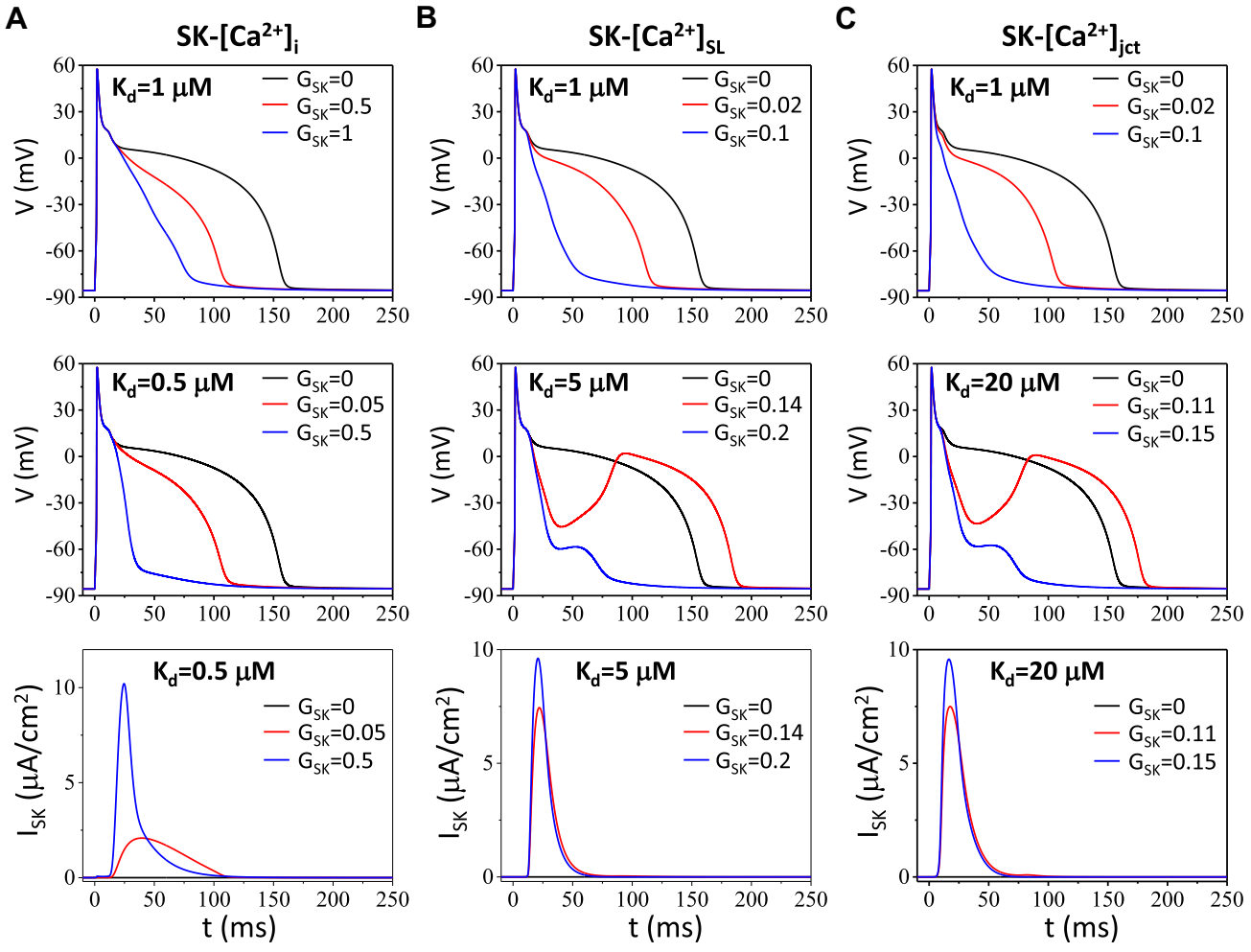

Figure 3 Effects of I_{SK} on AP morphology. Shown are APs and I_{SK} for different K_d and G_{SK} as labeled. The unit of G_{SK} is mS/μF. **A:** SK-$[Ca^{2+}]_i$. **B:** SK-$[Ca^{2+}]_{SL}$. **C:** SK-$[Ca^{2+}]_{jct}$. Ca^{2+}=calcium; AP=action potential; SK=small-conductance Ca^{2+} -activated K^+; I_{SK}=SK current; G_{SK}=maximum conductance of I_{SK}.

low, increasing G_{SK} decreases APD but the AP is always stable, independent of the SK channel localization. When SK channels sense Ca^{2+} in the bulk cytosolic compartment, changing K_d does not induce any complex AP dynamics. But when SK channels sense Ca^{2+} in the subsarcolemmal compartment or junctional cleft and K_d is large so that I_{SK} is spiky, APD alternans and more complex APD dynamics occur. Notably, these types of APD dynamics can also be induced by I_{to} as previously demonstrated in both computational and experimental studies.[20–23]

I_{SK} promotes J-wave syndrome and P2R

To examine whether I_{SK} can promote J-wave syndrome and P2R in tissue, we simulated 1D cables of 200 cells. Heterogeneity was simulated by increasing G_{SK} in half of the cable. The cable was paced from the endocardial side (top), and pseudo-ECGs were recorded on the epicardial side (bottom). When SK channels sense Ca^{2+} in the bulk cytosolic compartment (Figure 5A), increasing G_{SK} results in a large upright T wave but only has a small effect on elevating the J point. Changing K_d does not affect this behavior. When SK channels sense Ca^{2+} in the subsarcolemmal compartment or junctional cleft, if K_d is low, we also observed the same behavior. However, when K_d is large (Figures 5B and 5C), increasing G_{SK} elevates the J point and eventually promotes P2R. Note that in addition to elevation of the J point, the ECG becomes coved, which is a characteristic ECG behavior in Brugada syndrome.[24]

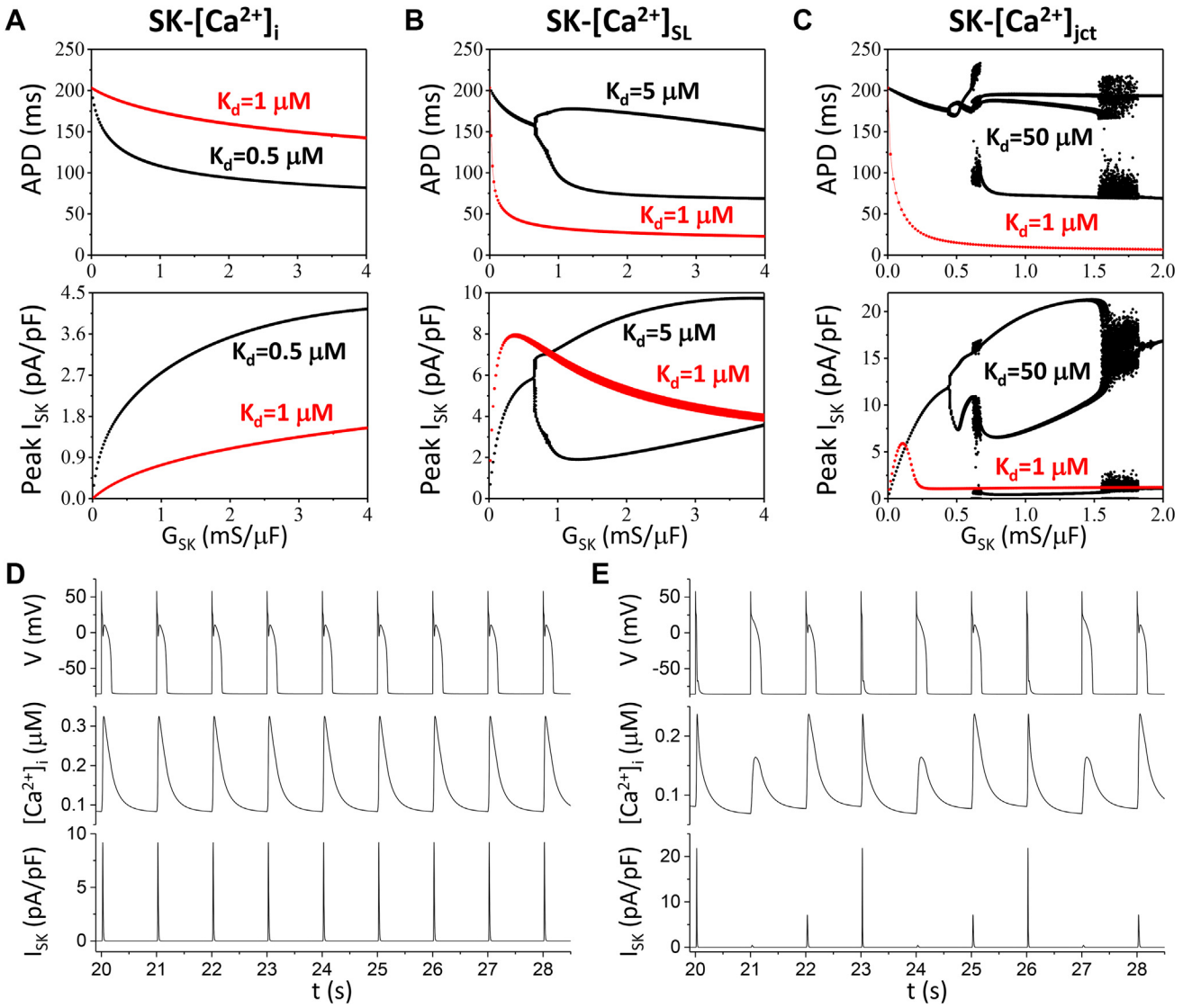

Figure 4 I_{SK} promotes complex APD dynamics. **A:** APD and peak I_{SK} vs G_{SK} for SK-$[Ca^{2+}]_i$ with $K_d = 0.5$ μM. **B:** APD and peak I_{SK} vs G_{SK} for SK-$[Ca^{2+}]_{SL}$ with $K_d = 5$ μM. **C:** APD and peak I_{SK} vs G_{SK} for SK-$[Ca^{2+}]_{jct}$ with $K_d = 50$ μM. In these panels, which are called bifurcation diagrams, APDs and peak I_{SK} from 60 beats are plotted for each G_{SK} values. The cells are paced with a pacing cycle length of 1000 ms. **D:** Voltage trace, $[Ca^{2+}]_i$, and I_{SK} for $G_{SK} = 0.25$ mS/μF for the case in panel C showing stable APD. **E:** Voltage trace, $[Ca^{2+}]_i$, and I_{SK} for $G_{SK} = 1$ mS/μF for the case in panel C showing a period-3 behavior (an ABCABC… pattern in AP morphology and APD). Similar period-3 patterns were observed in experiments by Lukas and Antzelevitch[22] and by Morita et al,[23] which were known to be caused by I_{to}. Ca^{2+} =calcium; AP=action potential; APD=action potential duration; SK=small-conductance Ca^{2+} -activated K^+; I_{SK}=SK current; G_{SK}=maximum conductance of I_{SK}; I_{to}=transient outward K^+ current.

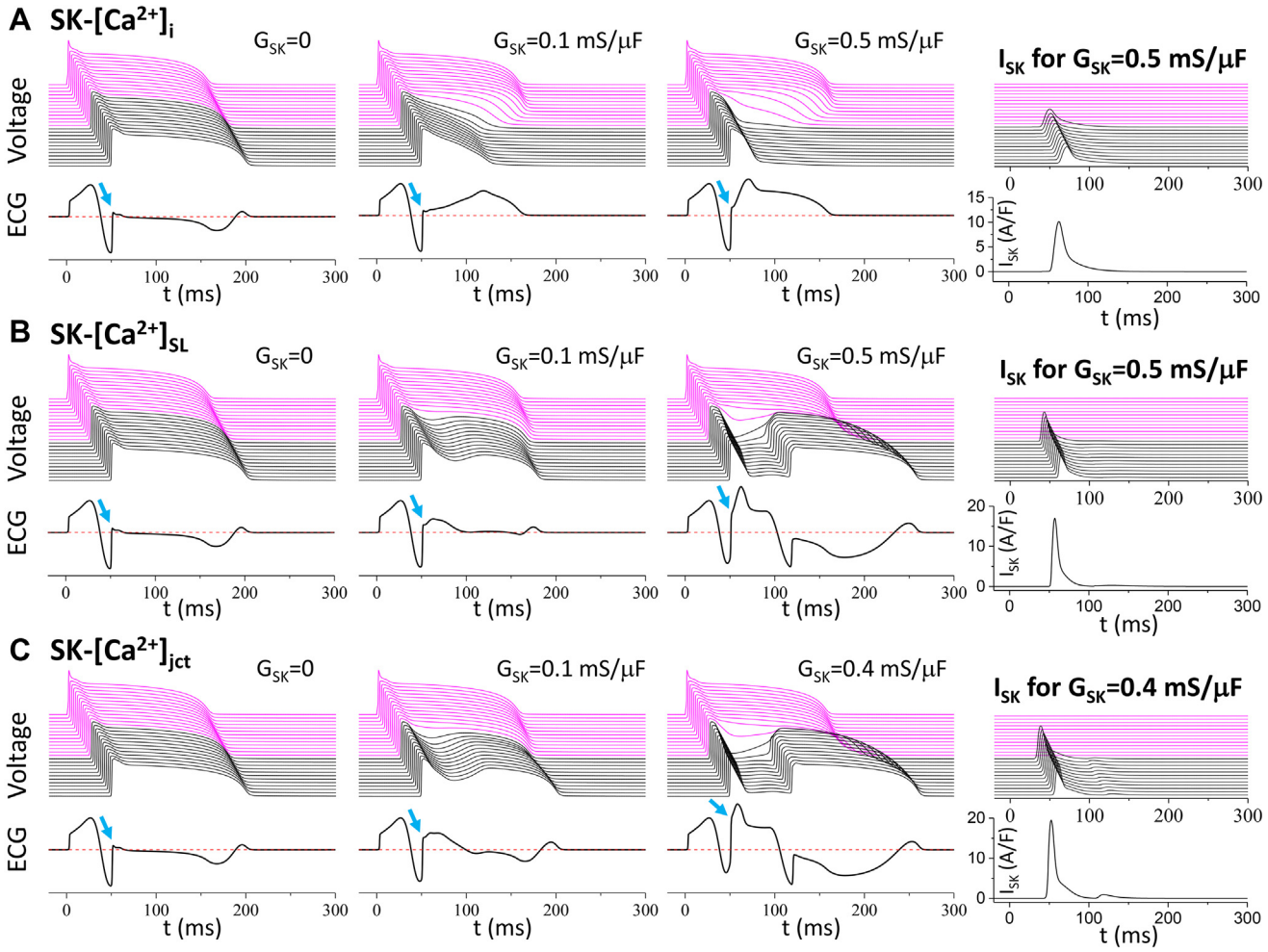

Figure 5 I_{SK} promotes J-wave elevation and P2R in a 1D cable with transmural heterogeneities. The cable length is 200 cells. G_{SK} was set to 0 in the first half of the cable (100 cells, *magenta*) and a nonzero value (as labeled in each panel) uniformly in the second half (*black*), which was then increased to increase the heterogeneity. For all the 1D cable simulations, a single stimulus was given (t = 0 ms) after the system reached the steady-state resting state. **Upper panels:** 3D (voltage-space-time) plots of voltage for 3 G_{SK} values. **Lower panels:** Pseudo-ECGs for each case. *Arrows* mark J points. The rightmost panels are the 3D plots of I_{SK} in the whole cable (upper) and plots of I_{SK} from 1 cell in the second half of the cable for the largest G_{SK} for each SK channel localization. **A:** SK channels sense the bulk cytosolic Ca^{2+}. K_d = 0.5 μM. **B:** SK channels sense the subsarcolemmal Ca^{2+}. K_d = 5 μM. **C:** SK channels sense the junctional Ca^{2+}. K_d = 20 μM. Ca^{2+} =calcium; P2R=phase 2 reentry; SK=small-conductance Ca^{2+} -activated K+; I_{SK}=SK current; G_{SK}=maximum conductance of I_{SK}; 1D=one-dimensional; 3D=three-dimensional.

We scanned G_{SK}, K_d, and τ_{SK} for P2R in the 1D cable model. When SK channels sense Ca^{2+} in the bulk cytosolic compartment, we cannot find P2R in this 1D cable model. When SK channels sense Ca^{2+} in the subsarcolemmal compartment (Figure 6A) or junctional cleft (Figure 6B), P2R can be observed for certain combinations of the 2 parameters. P2R is suppressed by increasing the activation time constant (Figures 6C and 6D).

Discussion

I_{SK} is present in both atrial and ventricular myocytes under normal and diseased conditions[2,3,6,8,9] and has been shown to be proarrhythmic in some settings and antiarrhythmic in others.[3,6,8,9,25,26] Recently, pharmacological I_{SK} activation with simultaneous Na^+ current suppression was shown to induce J-wave syndrome leading to ventricular arrhythmias in isolated rabbit hearts.[15] Although I_{to} is thought to play a key role in J-wave syndrome,[24] rabbits have almost no I_{to} at physiological heart rates because of its slow recovery from inactivation. This suggests that I_{SK} may have substituted for I_{to} because of its similar transient behavior as it tracks the intracellular Ca^{2+} transient. In this study, we used computer modeling to investigate the conditions under which I_{SK} may substitute for I_{to} to produce I_{to}'s hallmark arrhythmogenic features of spike-and-dome AP morphologies,[19–21] APD alternans, complex APD dynamics,[21–23] and P2R in cardiac tissue.[27–29] We show that when SK channels sense Ca^{2+} in the subsarcolemmal or junctional space where intracellular Ca^{2+} transient is spiky, I_{SK} rises and decays rapidly like I_{to} to promote J-wave syndrome and P2R.

Thus, our study provides a mechanistic insight into the experimental findings reported in isolated rabbit hearts that I_{SK} induced an arrhythmogenic J-wave syndrome, despite

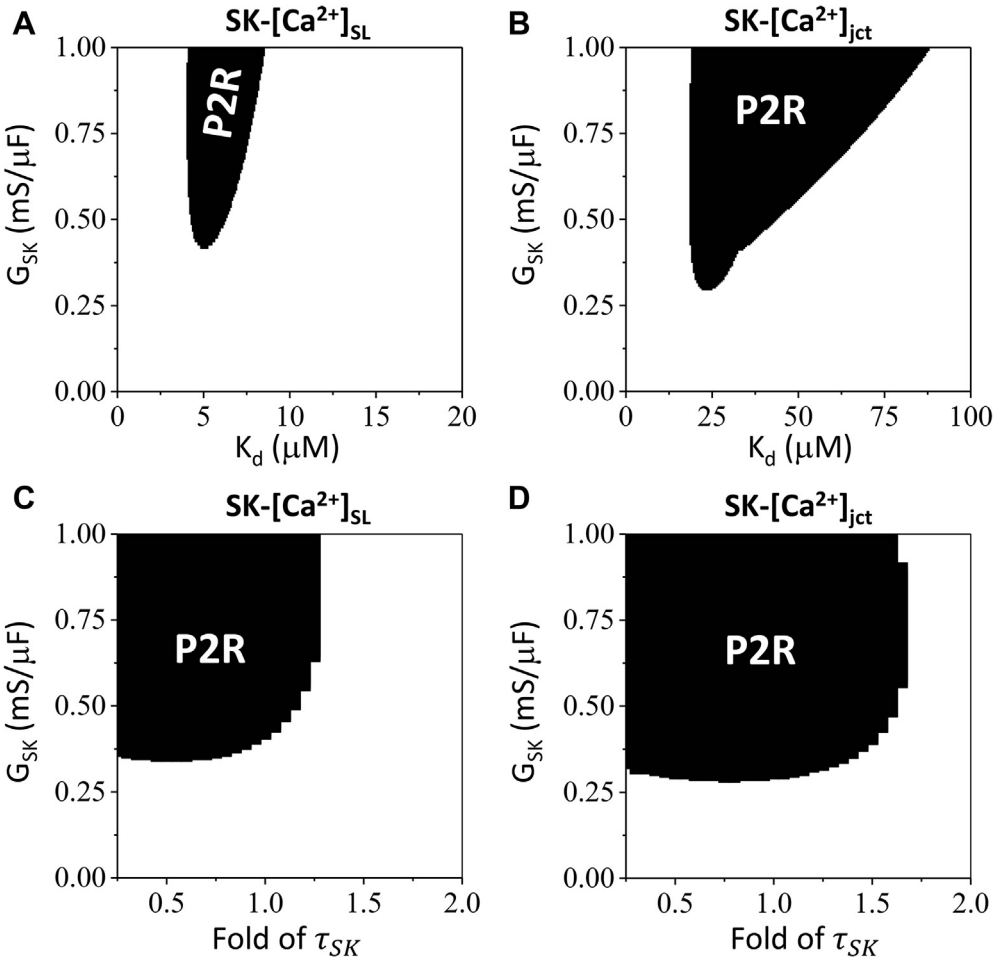

Figure 6 Effects of G_{SK}, K_d, and τ_{SK} on P2R. Shown are the P2R region in the combination of G_{SK} and K_d or G_{SK} and τ_{SK}. The same G_{SK} heterogeneities and pacing protocols as in Figure 5 were used. **A and C:** SK channels sense the subsarcolemmal Ca^{2+}. **B and D:** SK channels sense the junctional Ca^{2+}. Ca^{2+} =calcium; P2R=phase 2 reentry; SK=small-conductance Ca^{2+} -activated K^+; I_{SK}=SK current; G_{SK}=maximum conductance of I_{SK}.

the functional absence of significant I_{to}. The results from our study suggest that I_{SK} may synergize with I_{to} to cause all-or-none early repolarization and its arrhythmogenic consequences in human early repolarization syndromes such as Brugada syndrome. Most of the experimental studies of P2R have been carried out in canine hearts,[23,27,30] which

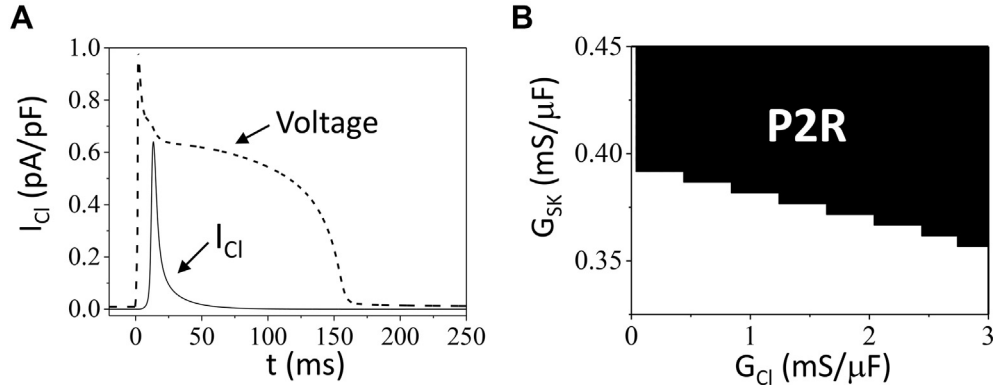

Figure 7 Effects of I_{Cl} on P2R. **A:** I_{Cl} (*solid line*) under an AP clamp condition (*dashed line*). We modified the I_{Cl} formulation (see Equation 74 in the Shannon-Bers article[18]) to $I_{Cl} = Fx_{Cl}\{G_{Cl}(V - E_{Cl})/[1 + (K_{dClCa}/[Ca]_C)^2]\}$,; that is, the Hill coefficient was changed from 1 to 2. The modification results in a spikier I_{Cl}, which agrees better with the I_{Cl} profile measured in experiments by Hegyi et al.[34] **B:** P2R region vs G_{SK} and G_{Cl} for SK channels sense the subsarcolemmal Ca^{2+}. The same G_{SK} heterogeneities and pacing protocols as in Figure 5 were used. The G_{Cl} value was uniformly increased in the whole cable. Ca^{2+} =calcium; P2R=phase 2 reentry; AP=action potential; SK=small-conductance Ca^{2+} -activated K^+; I_{SK}=SK current; G_{SK}=maximum conductance of I_{SK}; I_{Cl}=Ca^{2+} -activated chloride current; G_{Cl}=maximum conductance of I_{Cl}.

have an unusually high I_{to} density in the right ventricular epicardium. Experimentally, P2R has been much more difficult to induce in other species. For example, Park et al[31] attempted unsuccessfully to create a pig model of Brugada syndrome by engineering a human homologous loss-of-function *SCN5A* mutation, suggesting that I_{to} density in the pig was not high enough to recapitulate the Brugada syndrome phenotype. Therefore, in the setting of low or reduced I_{to}, activation of I_{SK} can promote J-wave syndrome and arrhythmias as in the rabbit experiments by Chen et al.[15]

Limitations

Several limitations are worth mentioning. Our simulations show that J-wave syndrome and P2R occur when SK channels sense Ca^{2+} in the junctional cleft or submembrane space such that they are transiently exposed to much higher Ca^{2+} concentrations when LCCs and ryanodine receptors open. However, our simulations also show that in order to produce a spiky enough I_{SK} for P2R, a higher K_d than experimentally estimated values in the submicromolar range is required.[3,10–13,17] K_d is the Ca^{2+} concentration at which I_{SK} is half-maximally activated, and thus a lower K_d indicates that the SK channel is more sensitive to Ca^{2+}. Since the Ca^{2+} concentration in the junctional cleft or subsarcolemmal space is much higher than 1 μM, I_{SK} amplitude may become saturated during the AP if K_d is in the submicromolar range (see Figure 2), blunting the spikiness too much for J-wave elevation and P2R to occur. However, experimental studies by Terentyev and coworkers[7,14] have shown that I_{SK} is much spikier than the bulk Ca^{2+} transient. Possible explanations are that (1) the actual K_d of SK channels in cardiac myocytes is higher than the measured apparent K_d assessed from the bulk Ca^{2+} concentration, perhaps because of the modulation of K_d by accessory proteins in the junctional cleft, or (2) I_{SK} is activated by submicromolar and then inactivated by supramicromolar Ca^{2+} concentrations in the submembrane space or junctional cleft. Evidence of inactivation or inhibition of I_{SK} at supramicromolar Ca^{2+} concentrations has been demonstrated in experiments.[14,32]

Furthermore, simulation results can be model specific, and we used only the Shannon-Bers model in this study. For example, our simulations could substantially overestimate K_d owing to the high Ca^{2+} concentrations in the junctional cleft or subsarcolemmal space of the model. In an experimental study of rabbit ventricular myocytes by Weber et al,[33] the measured Ca^{2+} concentration in the subsarcolemmal space is ~3- to 4-fold higher than the bulk cytosolic Ca^{2+} concentration. However, in the Shannon-Bers model, the subsarcolemmal Ca^{2+} concentration is 16-fold higher and the junctional cleft Ca^{2+} concentration is 300-fold higher than the bulk Ca^{2+} concentration (see Figure 2). This may result in a severalfold overestimation of the critical K_d for P2R.

Another limitation is that the I_{SK} conductance needed for P2R in our simulations is much higher than the experimentally measured values in ventricular myocytes under physiological or pathophysiological conditions.[3,14,34] This raises an issue whether I_{SK} was indeed responsible for P2R in the rabbit experiments by Chen et al.[15] One possibility is that in these experiments, I_{SK} was activated by drugs, which could be strong enough for P2R to occur. Another plausible explanation is that besides I_{SK}, there are other outward transient currents, which combine additively with I_{SK} to result in a total transient outward current that is strong enough to potentiate P2R. For example, experimental measurements show that the Ca^{2+}-activated chloride current (I_{Cl}) is also a spiky transient outward current[34,35] and is present in pig and rabbit ventricular myocytes. Therefore, I_{SK} alone may be not strong enough to induce P2R in the rabbit experiments by Chen et al, but it may combine with I_{Cl} to potentiate P2R. To demonstrate this possibility, we carried out the same 1D cable simulations as in Figures 5 and 6 and showed that increasing the maximum conductance of ICl (GCl) G_{Cl} decreased the G_{SK} threshold for P2R (Figure 7), indicating that the 2 currents are complementary to each other in promoting P2R. Similar to the limitations for the critical K_d discussed above, the critical current magnitude for P2R may also be model dependent, which needs to be validated by simulations of other models or by real experiments.

Nevertheless, the key property that I_{SK} is able to promote J-wave syndrome and ventricular arrhythmias is its spike-like behavior, which has indeed been shown in experimental measurements in ventricular myocytes.[7,14,34] The spikiness of I_{SK} may depend on many factors, such as Ca^{2+} transient profile, SK channel localization, K_d of SK channel activation, and activation time constant. The insights from our simulations provide a potential mechanism of J-wave syndrome and arrhythmogenesis in the experiments by Chen et al[15] and may be helpful for further experiments to reveal the roles of I_{SK} in promoting J-wave syndrome and arrhythmogenesis.

Conclusion

SK channels, which colocalize with LCCs in ventricular myocytes, may give rise to a spike-like I_{SK} because of SK channels sensing a spiky Ca^{2+} transient in the junctional cleft or subsarcolemmal space. I_{SK} can functionally play the role of I_{to} or combine together with other transient outward currents, such as I_{to} or I_{Cl}, to result in J-wave syndrome and potentiate ventricular arrhythmias by promoting T-wave alternans and P2R.

References

1. Adelman JP, Maylie J, Sah P. Small-conductance Ca^{2+}-activated K^+ channels: form and function. Annu Rev Physiol 2012;74:245–269.
2. Tuteja D, Xu D, Timofeyev V, et al. Differential expression of small-conductance Ca^{2+}-activated K^+ channels SK1, SK2, and SK3 in mouse atrial and ventricular myocytes. Am J Physiol Heart Circ Physiol 2005;289:H2714–H2723.
3. Chua SK, Chang PC, Maruyama M, et al. Small-conductance calcium-activated potassium channel and recurrent ventricular fibrillation in failing rabbit ventricles. Circ Res 2011;108:971–979.
4. Lu L, Zhang Q, Timofeyev V, et al. Molecular coupling of a Ca^{2+}-activated K^+ channel to L-type Ca^{2+} channels via α-actinin2. Circ Res 2007;100:112–120.
5. Zhang X-D, Coulibaly ZA, Chen WC, et al. Coupling of SK channels, L-type Ca^{2+} channels, and ryanodine receptors in cardiomyocytes. Sci Rep 2018;8:4670.

6. Chang PC, Turker I, Lopshire JC, et al. Heterogeneous upregulation of apamin-sensitive potassium currents in failing human ventricles. J Am Heart Assoc 2013; 2:e004713.
7. Terentyev D, Rochira JA, Terentyeva R, Roder K, Koren G, Li W. Sarcoplasmic reticulum Ca^{2+} release is both necessary and sufficient for SK channel activation in ventricular myocytes. Am J Physiol Heart Circ Physiol 2014;306:H738wH746.
8. Chang P-C, Hsieh Y-C, Hsueh C-H, Weiss JN, Lin S-F, Chen P-S. Apamin induces early afterdepolarizations and torsades de pointes ventricular arrhythmia from failing rabbit ventricles exhibiting secondary rises in intracellular calcium. Heart Rhythm 2013;10:1516–1524.
9. Zhang X-D, Lieu DK, Chiamvimonvat N. Small-conductance Ca^{2+}-activated K^+ channels and cardiac arrhythmias. Heart Rhythm 2015;12:1845–1851.
10. Hirschberg B, Maylie J, Adelman JP, Marrion NV. Gating of recombinant small-conductance Ca-activated K^+ channels by calcium. J Gen Physiol 1998;111:565–581.
11. Xia XM, Fakler B, Rivard A, et al. Mechanism of calcium gating in small-conductance calcium-activated potassium channels. Nature 1998;395:503.
12. Bildl W, Strassmaier T, Thurm H, et al. Protein kinase CK2 is coassembled with small conductance Ca^{2+}-activated K^+ channels and regulates channel gating. Neuron 2004;43:847–858.
13. Pedarzani P, Mosbacher J, Rivard A, et al. Control of electrical activity in central neurons by modulating the gating of small conductance Ca^{2+}-activated K^+ channels. J Biol Chem 2001;276:9762–9769.
14. Hamilton S, Polina I, Terentyeva R, et al. PKA phosphorylation underlies functional recruitment of sarcolemmal SK2 channels in ventricular myocytes from hypertrophic hearts [published online ahead of print February 16, 2029]. J Physiol, https://doi.org/10.1113/JP277618.
15. Chen M, Xu D-Z, Wu AZ, et al. Concomitant SK current activation and sodium current inhibition cause J wave syndrome. JCI Insight 2018;3:e122329.
16. Komendantov AO, Komendantova OG, Johnson SW, Canavier CC. A modeling study suggests complementary roles for GABAA and NMDA receptors and the SK channel in regulating the firing pattern in midbrain dopamine neurons. J Neurophysiol 2004;91:346–357.
17. Hirschberg B, Maylie J, Adelman JP, Marrion NV. Gating properties of single SK channels in hippocampal CA1 pyramidal neurons. Biophys J 1999; 77:1905–1913.
18. Shannon TR, Wang F, Puglisi J, Weber C, Bers DM. A mathematical treatment of integrated Ca dynamics within the ventricular myocyte. Biophys J 2004; 87:3351–3371.
19. Greenstein JL, Wu R, Po S, Tomaselli GF, Winslow RL. Role of the calcium-independent transient outward current I_{to1} in shaping action potential morphology and duration. Circ Res 2000;87:1026–1033.
20. Clancy CE, Rudy Y. Na^+ channel mutation that causes both Brugada and long-QT syndrome phenotypes: a simulation study of mechanism. Circulation 2002; 105:1208–1213.
21. Landaw J, Qu Z. Memory-induced nonlinear dynamics of excitation in cardiac diseases. Phys Rev E 2018;97:042414.
22. Lukas A, Antzelevitch C. Differences in the electrophysiological response of canine ventricular epicardium and endocardium to ischemia: role of the transient outward current. Circulation 1993;88:2903–2915.
23. Morita H, Zipes DP, Lopshire J, Morita ST, Wu J. T wave alternans in an in vitro canine tissue model of Brugada syndrome. Am J Physiol Heart Circ Physiol 2006; 291:H421–H428.
24. Antzelevitch C, Yan G-X, Ackerman MJ, et al. J-wave syndromes expert consensus conference report: emerging concepts and gaps in knowledge. Heart Rhythm 2016;13:e295–e324.
25. Kennedy M, Bers DM, Chiamvimonvat N, Sato D. Dynamical effects of calcium-sensitive potassium currents on voltage and calcium alternans. J Physiol 2017; 595:2285–2297.
26. Morotti S, Koivumäki JT, Maleckar MM, Chiamvimonvat N, Grandi E. Small-conductance Ca^{2+}-activated K^+ current in atrial fibrillation: both friend and foe. Biophys J 2016;110:274a.
27. Lukas A, Antzelevitch C. Phase 2 reentry as a mechanism of initiation of circus movement reentry in canine epicardium exposed to simulated ischemia. Cardiovasc Res 1996;32:593–603.
28. Maoz A, Christini DJ, Krogh-Madsen T. Dependence of phase-2 reentry and repolarization dispersion on epicardial and transmural ionic heterogeneity: a simulation study. Europace 2014;16:458–465.
29. Bueno-Orovio A, Cherry EM, Evans SJ, Fenton FH. Basis for the Induction of tissue-level phase-2 reentry as a repolarization disorder in the Brugada syndrome. Biomed Res Int 2015;2015:197586.
30. Aiba T, Shimizu W, Hidaka I, et al. Cellular basis for trigger and maintenance of ventricular fibrillation in the Brugada syndrome model: high-resolution optical mapping study. J Am Coll Cardiol 2006;47:2074–2085.
31. Park DS, Cerrone M, Morley G, et al. Genetically engineered *SCN5A* mutant pig hearts exhibit conduction defects and arrhythmias. J Clin Invest 2015; 125:403–412.
32. Soh H, Park C-S. Localization of divalent cation-binding site in the pore of a small conductance Ca^{2+}-activated K^+ channel and its role in determining current-voltage relationship. Biophys J 2002;83:2528–2538.
33. Weber CR, Piacentino V III, Ginsburg KS, Houser SR, Bers DM. Na^+-Ca^{2+} exchange current and submembrane [Ca^{2+}] during the cardiac action potential. Circ Res 2002;90:182–189.
34. Hegyi B, Bossuyt J, Griffiths LG, et al. Complex electrophysiological remodeling in postinfarction ischemic heart failure. Proc Natl Acad Sci U S A 2018; 115:E3036–E3044.
35. Verkerk AO, Veldkamp MW, Baartscheer A, et al. Ionic mechanism of delayed afterdepolarizations in ventricular cells isolated from human end-stage failing hearts. Circulation 2001;104:2728–2733.